European Journal of Pharmaceutical Sciences 215 (2025) 107344

Contents lists available at ScienceDirect

European Journal of Pharmaceutical Sciences

journal homepage: www.elsevier.com/locate/ejps

Preclinical evaluation of Manganese-52 labelled cyclodextrin: a prostaglandin E2 affine imaging probe

Renáta Adél Dienes [a,b,1], Lili Anna Komor [b,1], Judit P. Szabó [b], András Berzi [b], Miklós Emri [b], Dezső Szikra [b], Anikó Fekete [b], Gábor Opposits [b], István Józsai [b], István Kertész [b], Ferenc Fenyvesi [c], György Trencsényi [a,b], István Hajdu [b,2], Zita Képes [a,b,2,*]

[a] Gyula Petrányi Doctoral School of Clinical Immunology and Allergology, Faculty of Medicine, University of Debrecen, Nagyerdei St. 98 H-4032 Debrecen, Hungary
[b] Division of Nuclear Medicine and Translational Imaging, Department of Medical Imaging, Faculty of Medicine, University of Debrecen, Nagyerdei St. 98 H-4032 Debrecen, Hungary
[c] Department of Molecular and Nanopharmaceutics, Faculty of Pharmacy, University of Debrecen, Rex Ferenc St. 1 H-4002 Debrecen, Hungary

ARTICLE INFO

Keywords:
Manganese-52
Positron emission tomography
Pancreatic cancer
Preclinical
Prostaglandin E2 (PGE2)
Randomly methylated β-cyclodextrin (RAMEB)

ABSTRACT

Prostaglandin E2 (PGE2) is implicated in several tumor-related biological processes, making it a promising biomarker for molecular imaging. In nuclear medicine, radiolabelled cyclodextrins have emerged as potential probes to target PGE2 in various cancer types. Hereafter, we aimed to specify the pharmacokinetics of a novel Manganese-52-labelled randomly methylated β-cyclodextrin ([^{52}Mn]Mn-DOTAGA-RAMEB) by performing multiple time-point positron emission tomography and *ex vivo* biodistribution studies in PGE2 positive BxPC-3 pancreatic adenocarcinoma xenografts. In line with the *ex vivo* findings, [^{52}Mn]Mn-DOTAGA-RAMEB showed early and specific tumor uptake (30 and 60 min after injection), followed by rapid wash-out and renal clearance. Our experimental data demonstrate the feasibility of ^{52}Mn-labelled RAMEB cyclodextrin to identify PGE2 expressing tumors, although further pharmacokinetic optimization is required to enhance tumor retention and fully exploit its diagnostic potential.

1. Introduction

Even though major gains have been ongoing in the field of clinical oncology over the past decades, malignant diseases still continue to challenge the health and economic systems of all countries worldwide. As therapeutic success and patient outcomes highly depend on early diagnosis, the quest for more specific and sensitive imaging probes is in the forefront of oncological research.

Prostaglandin E2 (PGE2), derived from cyclooxygenase-2 (COX-2) and microsomal prostaglandin E2 synthase-1 (mPGES-1) (Tong et al., 2018), is closely associated with tumorigenesis (Finetti et al., 2020). Via E-type prostanoid receptor (EP 1–4) activation, PGE2 has been demonstrated to induce several tumor-related biological processes such as angiogenesis, proliferation, invasion, or apoptosis inhibition (Hanahan and Weinberg, 2011; Niu et al., 2019; Santisoet al., 2024). In addition, the overexpression of the main metabolic enzymes and increased PGE2 levels in various cancer types (e.g.: breast cancer (Half et al., 2002), prostate cancer (Finetti et al., 2015), melanoma (Panza et al., 2016), or non-small cell lung cancer (Fang et al., 2003)) suggests its use as a diagnostics biomarker and a therapeutic target as well.

Since cyclodextrin molecules (Cyd) show outstanding complex forming capability with PGE2 (Hirayama et al., 1984; Sauer et al., 2017), our research team hypothesized that these oligosaccharides would be perfectly suitable for the construction of PGE2-targeting molecular and radiopharmaceutical agents (Hajdu et al., 2019; Trencsényi et al., 2020). *Hajdu and colleagues* were the first to synthesize a radiolabelled beta-Cyd derivative ([^{68}Ga]Ga-NODAGA-HPβCD; hydroxypropyl-β-Cyd) and publish preliminary positron emission tomography (PET) results on its pharmacokinetics and *in vivo* biodistribution (Hajdu et al., 2019). To test the feasibility of Cyd-based radiopharmaceuticals in the detection of PGE2 expressing malignancies, a series of preclinical PET experiments using [^{68}Ga]Ga-NODAGA-RAMEB (randomly methylated β-Cyd) or [^{68}Ga]Ga-NODAGA-HPβCD was performed in several

* Corresponding author at: Division of Nuclear Medicine and Translational Imaging, Department of Medical Imaging, Faculty of Medicine, University of Debrecen, Nagyerdei St. 98 H-4032 Debrecen, Hungary.
E-mail address: kepes.zita@med.unideb.hu (Z. Képes).
[1] These authors contributed equally to the present work.
[2] These authors contributed equally to the present work.

https://doi.org/10.1016/j.ejps.2025.107344
Received 3 July 2025; Received in revised form 8 September 2025; Accepted 21 October 2025
Available online 21 October 2025

Abbreviation list

COX-2	cyclooxygenase-2 enzyme
CPM	counts per minute
Cyd	cyclodextrin
DMEM	Dulbecco's modified Eagle medium
DOTAGA	1,4,7,10-tetraazacyclododecane,1-(glutaric acid)-4,7,10-triacetic acid
EP	prostaglandin E receptor
HPLC	high-performance liquid chromatography
HPβCD	hydroxypropyl-β-cyclodextrin
mPGES-1	microsomal prostaglandin E2 synthase-1
MS	mass spectrometry
NH_2-RAMEB	6-Monodeoxy-6-monoamino-randomly-methylated-beta-cyclodextrin hydrochloride
PET	positron emission tomography
PGE2	prostaglandin E2
RAMEB	randomly methylated β-cyclodextrin
SCID	severe combined immunodeficient
SUV	Standardized Uptake Value
T/M	tumor-to-muscle ratio
TAC	time-activity-curve
VOI	volume of interest

tumor models with varying PGE2 expression profile such as HT1080 (human fibrosarcoma), A20 (mouse B cell lymphoma), PancTu-1 and BxPC3 (human pancreas adenocarcinoma), B16F10 (mouse melanoma), Ne/De (rat mesoblastic nephroma) and He/De (rat hepatocellular carcinoma) (Szabó et al., 2023; Trencsényi et al., 2020). Based on increased Cyd uptake in tumors with high PGE2 expression and negligible background activity, our team first ever confirmed the PGE2 selectivity of these radioactive probes (Szabó et al., 2023; Trencsényi et al., 2020). In addition, labelling with alternative isotopes such as Bismuth-213 (^{213}Bi) also seemed to be optimal for Cyd-based therapeutic applications (Csige et al., 2022).

In addition, regardless of their diagnostic potential (Csige et al., 2022; Hajdu et al., 2019; Szabó et al., 2023; Trencsényi et al., 2020), the future progression of both ^{68}Ga, - and ^{213}Bi -labelled Cyds from bench to bedside may be limited by the short longevity of these isotopes ($T_{1/2}$ = 68 and 45.6 min for ^{68}Ga and ^{213}Bi; respectively) complicating delayed imaging and logistics (Ahenkorah et al., 2021; Giesel et al., 2021). In contrast, using longer-lived Manganese-52 (^{52}Mn; $T_{1/2}$ = 5.59 days, β^+=242 KeV; (Pyles et al., 2023)) for radiolabelling could not only ensure imaging beyond the conventional time-window (Graves et al., 2015), but may also bypass transport challenges. Inspired by these facts, in our prior work, a novel, ^{52}Mn-labelled RAMEB derivative was constructed ([^{52}Mn]Mn-DOTAGA-RAMEB) and evaluated for diagnostic applications using B16F10 melanoma models (Képes et al., 2024). Showing meaningful tumor tracer accumulation, PET images recorded 1 h post-injection definitely indicated the tumor-homing ability of [^{52}Mn]Mn-DOTAGA-RAMEB; however, faint uptake at later time-points warrant further pharmacokinetic investigations.

For this reason, in the present work we aimed to better capture the totality of the pharmacokinetics of [^{52}Mn]Mn-DOTAGA-RAMEB by performing multi-time point PET imaging and *ex vivo* studies with PGE2 positive xenografts and healthy counterparts. We deliberately chose the BxPC-3 pancreatic adenocarcinoma model for tumor establishment, given its well documented ability to produce high levels of PGE2 (Yip-Schneider et al., 2000; Takahashi et al., 2015), providing a suitable system to assess the behaviour of this probe in imaging settings. We hypothesize that additional pharmacokinetical characterization may further support the added value of ^{52}Mn-labelled compounds in oncological PET diagnostics.

2. Materials and methods

2.1. Chemistry

2.1.1. Chemicals

6-Monodeoxy-6-monoamino-randomly-methylated-beta-cyclodextrin hydrochloride (NH_2-RAMEB) was produced by CycloLab Ltd. (Budapest, Hungary). The bifunctional chelator p-NCS-Bz-DOTA-GA (DOTAGA) was purchased from CheMatech (Cat. No.:C115) (Dijon, France). Chromium powder (60 mesh, 99.99 % purity) was obtained from Thermo Fisher Scientific Ltd. (Waltham, Massachusetts, USA). The ^{52}Mn radioisotope was prepared in the GE PETtrace cyclotron at the Division of Nuclear Medicine and Translational Imaging, Department of Medical Imaging, Faculty of Medicine, University of Debrecen (Debrecen, Hungary). Analytical grade AG 1-X8 anion exchange resin (200 - 400 mesh) was purchased from Bio-Rad Laboratories Inc. (Hercules, California, USA). Ultra-pure (u.p.) HCl was the product of Merck Ltd. (Budapest, Hungary). Ultrapure water (Sigma-Aldrich Ltd., Budapest, Hungary) was used for the preparation of all solvents and mixtures during this research. All other chemicals were purchased from VWR International Ltd. (Debrecen, Hungary) and Sigma-Aldrich Ltd. (Budapest, Hungary), and they were used without further purification.

2.1.2. Conjugation of DOTAGA to NH2-RAMEB

The DOTAGA bifunctional chelator was attached to the amino group of NH2-RAMEB according to the protocol described by Csige et al. (Csige et al., 2022). Briefly, 20 mg (16 μmol) of NH_2-RAMEB was dissolved in 1.5 mL of water and this aqueous solution was stirred at 4 °C for 15 min. After DOTAGA (m = 11 mg, n = 16 μmol) was added to the cooled NH_2-RAMEB solution, the pH of the reaction mixture was adjusted to 8.3 by dropwise addition of DIPEA. The reaction mixture was then stirred at room temperature for 24 h. The product (DOTAGA-RAMEB) was lyophilized, redissolved in water and purified on a Knauer HPLC system. The purity of DOTAGA-RAMEB was determined using a KNAUER RP-HPLC system, and the molecular weight of the product was confirmed with high-resolution mass spectrometry (MS). Finally, DOTAGA-RAMEB was dissolved in u. p. water to produce a stock solution (c = 3 mM) for subsequent radiolabelling reactions.

2.1.3. Production and purification of 52Mn isotope

The ^{52}Mn isotope was generated through the ^{52}Cr(p,n)^{52}Mn reaction, by proton irradiation with a 20 MeV beam on a natural Cr/Mg powder mixture target using a Cr target of 40 mg. After 1 h irradiation, the yield of the ^{52}Mn was approx. 90 MBq. The purification of the radionuclide was performed based on the method of Fonslet et al. (Fonslet et al., 2017). The process was developed on the solid phase extraction of manganese from acid/organic solvent mixtures. After a 24 h decay period, the irradiated target was placed in a plastic vial and using 2 mL of 3 M u. p. HNO_3 Mg was dissolved. Afterwards, followed by the removal of HNO_3, the Cr powder was washed 2 times with 5 mL of u. p. H_2O and was dissolved in concentrated HCl (V = 3 mL) in a heating block at 95 °C for approx. 30 min. The solution was concentrated to ~1.5 mL with nitrogen flow and was diluted with 48.5 mL of absolute ethanol. Then the mixture was moved onto a 300 mg AG® 1-X8 extraction column, which was preconditioned with 6 mL of 3 v/v % u. p. HCl in absolute ethanol. The column was washed using approx. 20 mL of 3 v/v % u. p. HCl in absolute ethanol, and the ^{52}Mn isotope was eluted with 0.5 mL of 0.1 M HCl. The ^{5}2Mn solution was concentrated to dryness in a heating block at 95 °C with nitrogen flow, redissolved in 300 μL of concentrated u. p. HCl, and then diluted to 10 mL with absolute ethanol. The process was repeated two more times, with the difference that the second and the third time, 200 mg and 100 mg of AG® 1-X8 resin was used; respectively. Finally, ~60 MBq ^{52}Mn isotope was eluted with 200 μL of 0.1 M HCl and used for radiolabelling purposes.

2.1.4. [^{52}Mn]Mn-DOTAGA-RAMEB radiolabelling

Using precursor DOTAGA-RAMEB, radiolabelling was carried out based on a protocol previously described by Képes et al. (Képes et al., 2024). Briefly, 100 μL of ^{52}Mn in a 0.1 M HCl solution was mixed with 500 μL of sodium-acetate buffer ($c = 2$ M) to adjust the solution to pH 7.0. Subsequently, 10 μL of DOTAGA-RAMEB ($c = 3$ mM) from stock solution was added to the reaction mixture. The sample was then heated at 95 °C for 10 min and allowed to cool at room temperature for 5 min.

Formulation and purification were performed using a Light C18 Sep-Pak Cartridge (Waters Ltd., Budapest, Hungary). After elution with 96 % EtOH, the radiolabelled product ([^{52}Mn]Mn-DOTAGA-RAMEB) was evaporated to dryness and was redissolved in isotonic NaCl solution. Quality control (iTLC chromatography) was followed by the sterile filtration of [^{52}Mn]Mn-DOTAGA-RAMEB, which was then diluted with isotonic saline prior to animal experiments.

2.2. Biological characterization

2.2.1. Cell culturing

BxPC-3 (PGE2 positive) human pancreas adenocarcinoma cells (CRL-168, American Type Culture Collection (ATCC), Manassas, VA, USA) were cultured as recommended by the distributor. Briefly, cells were cultivated in Dulbecco's Modified Eagle medium (DMEM, Merck Life Science Ltd., Budapest, Hungary) at 37 °C in a 5 % CO_2 incubator. Followed by viability assessment with trypan blue staining, cells with a viability exceeding 90 % were used for *in vivo* studies.

2.2.2. Animal housing

Healthy control ($n = 12$) and BxPC-3 tumor-bearing ($n = 15$) CB17 severe combined immunodeficient (SCID) mice obtained from Innovo Ltd. (Isaszeg, Hungary) were housed in pathogen-free, individually ventilated cages (IVC; Techniplast, Italy) under automatically controlled 12-hour day/night cycles at a temperature of 26±3 °C and 52±10 % humidity. Sterile semi-synthetic rodent food (sterile VRF1 rodent feed; Akronom Ltd., Budapest, Hungary) and sterile drinking water were available for the study mice ad libitum. All animal experiments were approved by the Ethics Committee for Animal Experiments of the University of Debrecen (license number: 16/2020/DEMÁB) and have been performed in accordance with the general animal welfare regulations of the European Union.

2.2.3. Tumor generation

Prior to tumor induction, isoflurane-based anaesthesia (3 % Forane, 0.4 L/min O_2, 1.4 L/min N_2O) was applied using a small animal inhalation anaesthesia machine (TEC3 Eickemeyer Research isoflurane vaporizer; Ghislandi and Társai Ltd., Budapest, Hungary). To establish tumor models, a maximum of 5×10^6 BxPC-3 human pancreas adenocarcinoma cells in 100 μL of 0.9 % saline solution were injected into the left shoulder area of the study mice. After tumor induction, tumor growth was monitored using caliper measurements. Tumor volume (V, mm^3) was calculated as $V=(L*W^2)/2$ where V is the tumor volume (mm^3), L is the tumor length (mm), and W is the tumor width (mm). The xenotransplants were ready for miniPET imaging 12±1 days post tumor cell transplantation when the tumors had grown to an average volume of 98±5 mm^3.

2.2.4. In vivo PET imaging

To explore the pharmacokinetics of [^{52}Mn]Mn-DOTAGA-RAMEB in detail, after the tail vein injection of the BxPC-3 tumor-bearing mice with 4.1 ± 0.37 MBq radiotracer (in 150 μL saline solution), dynamic (0–240 min) PET imaging was done, that was followed by 10-minute static acquisition at different time-points/intervals (10, 20, 30, 60, 90, 180 and 240 min) post-injection based on previously published protocols (Képes et al., 2024). To minimize potential bias, mice were randomly assigned to the respective time points. Animal numbers for each experiment are indicated in the respective data tables, and representative figures. PET images were recorded using the preclinical MiniPET-II scanner of the Division of Nuclear Medicine and Translational Imaging, Department of Medical Imaging, Faculty of Medicine, University of Debrecen (Debrecen, Hungary). We ensured that all mice were under anaesthesia using 3 % Aerrane (Baxter Hungary Ltd., Budapest, Hungary, OGYI-T-08,993) 0.4 L/min O_2 and 1.2 L/min N_2O during tracer injection and PET acquisition, and waked up normally after imaging.

2.2.5. PET data assessment

For quantitative image analysis, volumes of interests (VOIs) were manually placed over the subcutaneously growing BxPC-3 tumors on each decay-corrected transaxial PET slice using the BrainCad image analysis software. Based on the following formula, the mean radiopharmaceutical concentration (standardized uptake value/SUV) of each VOI was calculated: SUV=VOI activity (Bq/mL)/[injected activity (Bq)/animal weight (g)], assuming a density of 1 g/mL. Tumor-to-non-target (T/M) ratios were determined from the tumor SUVmean and the SUV-mean of the background muscle tissue.

2.2.6. Ex vivo organ distribution

For organ distribution studies all study mice were anaesthetized, *iv.* administered with 3.1 MBq±0.23 of [^{52}Mn]Mn-DOTAGA-RAMEB via the lateral tail vein, and then sacrificed at 30, - 60, 180, and, - 240 min after tracer administration. Blood was taken from the heart using a syringe, and then tissues of the major organs/tissues and the tumors were removed, weighed wet and measured for radioactivity with a calibrated gamma counter: liver, spleen, kidneys, stomach, small and large intestines, pancreas, gall bladder, lung, heart, brain, salivary gland, bone (femur), and fat, muscle tissue and urine. The counts per minute (CPM) values of all samples were converted to the percent of injected activity per gram of tissue (%ID/g) and the uptake figures were presented as mean %ID/*g*±SD. Animal numbers for each experiment are presented in the respective data tables, and representative figures.

2.2.7. Statistical analyses

Quantitative data were presented as mean ± standard deviation (SD). Statistical analysis was performed with MedCalc 18.5 commercial software package (MedCalc Software, Mariakerke, Belgium). Significance was determined using Student's two-tailed *t*-test, two-way ANOVA, and Mann-Whitney rank-sum tests. Statistical significance was defined as $P < 0.01$.

3. Results and discussion

3.1. Chemistry

The conjugation reaction between the RAMEB cyclodextrin molecule and the DOTAGA bifunctional chelator that resulted in DOTAGA-RAMEB precursor enabled radiolabelling RAMEB with ^{52}Mn radioisotope. The final product was purified using high-performance liquid chromatography (HPLC), and products with purity exceeding 98 % were registered. The yield of the synthesis was 81 %.

The whole radiolabelling procedure including labelling, purification and formulation was performed manually with an average 20-min reaction time for each step. ^{52}Mn was observed to be rapidly chelated by DOTAGA-RAMEB in pH 7 and at 95 °C. [^{52}Mn]Mn-DOTAGA-RAMEB was formed with >99 % conversion based on iTLC chromatography.

3.2. In vivo studies in BxPC-3 tumor-bearing mice

3.2.1. Visual assessment

[^{52}Mn]Mn-DOTAGA-RAMEB biodistribution and tumor uptake were assessed by dynamic and static microPET imaging in PGE2 positive BxPC-3 xenografts. Multiple-time point static microPET scans are shown in Fig. 1 **Panel A** with an overview of uptake kinetics from 0 to 240 min

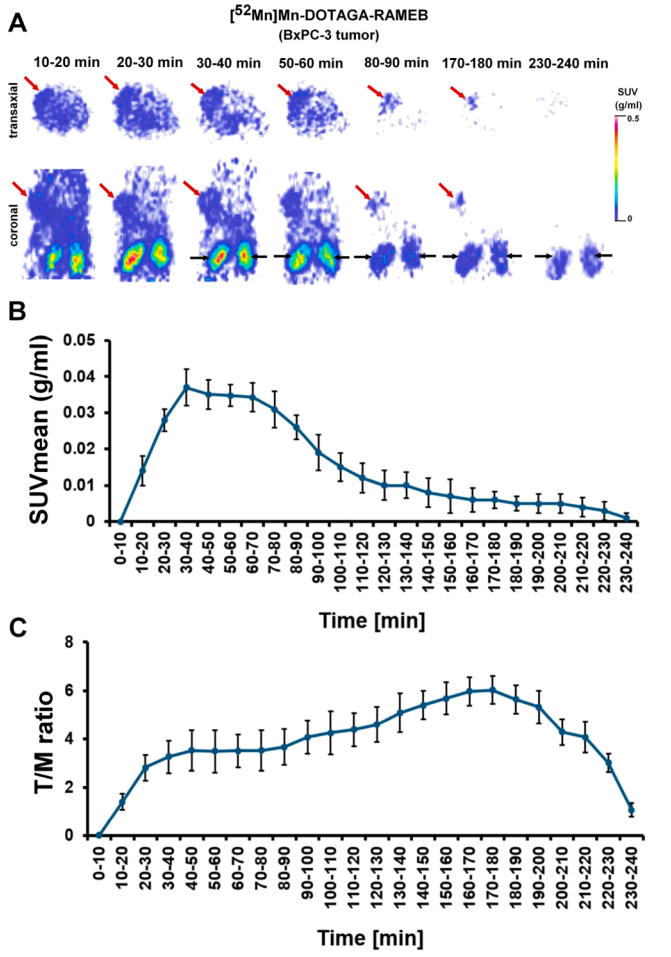

Fig. 1. Representative micro-PET images and time-activity curves. A series of transaxial (upper row) and coronal (lower row) [^{52}Mn]Mn-DOTAGA-RAMEB PET images of BxPC-3 tumor-bearing CB17 SCID mice (Panel A), the subcutaneously growing BxPC-3 tumors are indicated with red arrows. Dynamic time-activity curves of [^{52}Mn]Mn-DOTAGA-RAMEB in BxPC-3 tumors (Panel B). Tumor-to-muscle ratios of [^{52}Mn]Mn-DOTAGA-RAMEB for 240BxPC-3min (Panel C). PET: positron emission tomography, SUV: standardized uptake value, T/M: tumor-to-muscle ratio.

in Fig. 1, **Panel B**. Corresponding SUV values for the accumulated radioactivity and T/M ratios are displayed in Table 1.

In BxPC-3 tumor-bearing mice, [^{52}Mn]Mn-DOTAGA-RAMEB was absorbed highly by the tumor at 30 min and 60 min after injection, however, the uptake sharply decreased until the 240 min time point (as seen in Fig. 1 **Panel A**). In line with former findings, these results confirm the potential of radiolabelled cyclodextrin derivatives for the PET imaging of PGE2 expressing tumors (Hajdu et al., 2019; Képes et al., 2024; Szabó et al., 2023; Trencsényi et al., 2020), and highlight the relevance of ^{52}Mn as an attractive alternative radionuclide for the de novo construction of PET agents that is also similar to recently published data (Képes et al., 2024). Considering the PGE2 positivity of BxPC-3 tumors (Szabó et al., 2023; Takahashi et al., 2015), our experiences further strengthened the PGE2 targeting ability of RAMEB cyclodextrin, consistent with previous reports (Hajdu et al., 2019; Sauer et al., 2017; Trencsényi et al., 2020). The binding selectivity of RAMEB for PGE2 has already been confirmed for example by resin binding assays which revealed significantly higher radioactivity retention on PGE2-conjugated resins compared to unmodified samples, as well as by *in vivo* PET studies using co-injection of excess PGE2 (Trencsényi et al., 2020). Nevertheless, increased RAMEB uptake likely reflects strong tumor PGE2 expression of BxPC-3 tumors, capturing the totality of binding mechanisms including potential off-target sites requires additional studies.

Table 1
Quantitative PET data of [^{52}Mn]Mn-DOTAGA-RAMEB in BxPC-3 tumor-bearing CB17 SCID mice.

	SUVmean	T/M ratio
30 min	0.037±0.005	2.80±0.53
60 min	0.034±0.004	3.49±0.67
90 min	0.019±0.005	4.06±0.69
180 min	0.006±0.003	5.64±0.59
240 min	0.001±0.001	1.06±0.28

PET: positron emission tomography,.
SCID: severe combined immunodeficient,.
T/M: tumor-to-muscle ratio.

3.2.2. *Quantitative static and dynamic PET assessment*

Even though [^{52}Mn]Mn-DOTAGA-RAMEB performed well in tumor identification at early acquisition time points with peak SUV values 30 min post-injection (SUVmean: 0.037±0.005), on delayed scans hardly any radioactivity could be registered (SUVmean: 0.019±0.005, 0.006 ±0.003 and 0.001±0.001 at 90, 180 and 240 min after tracer injection; respectively; Table 1). Our finding was somewhat similar to the results of Képes et al. who reported a similar uptake tendency for [^{52}Mn]Mn-DOTAGA-RAMEB (Képes et al., 2024), although the SUV values differed significantly at corresponding time points. Followed by a peak uptake 1 h post-injection, static PET scans on B16F10 melanoma tumors showed rapid tracer clearance until termination (60 min SUVmean 0.06±0.01, 240 min SUVmean 0.02±0.01 and 3 days SUVmean: 0.01±0.01; (Képes et al., 2024)). Differences between B16F10 and BxPC-3 uptake are likely due to variations in tumor biology and PGE2/EP expression. Based on the long half-life of ^{52}Mn (approx. 5.5 days), however, prolonged retention was expected even at delayed imaging time points, therefore, to delve more into tracer accumulation kinetics additional dynamic PET imaging from 0–240 min was performed (Fig. 1, **Panel B**).

Assessing the time-activity-curve (TAC), the tumors were clearly delineated from the background already at the 30–40 min frame fusion (Fig. 1, **Panel B**) showing a peak SUV of 0.037±0.005 half an hour post-injection (Fig. 1, **Panel B**). Similarly to what was observed in Fig. 1, **Panel A**, followed by a meaningful tracer uptake within 0–60 min, the TAC also indicated steady declining tumor radioactivity, reaching an equilibrium around 160-min post-injection (SUVmean: 0.007±0.005). Comparisons with the TAC of ^{68}Ga-labelled DOTAGA-RAMEB show similar decreasing trends in BxPC-3 tumors (Csige et al., 2022), nevertheless, its wash-out kinetics seemed rather gradual. Followed by a gradual drop in tumor accumulations within the 3–50-min time-window ([^{68}Ga]Ga-DOTAGA-RAMEB SUVmean: 0.36±0.04 and 0.20±0.04 3 and 50 min post-injection; respectively) an equilibrium was achieved resulting in intensive tumor activity and good contrast even at the 90-min time-point. Despite the chelator change, research by *Trencsényi and co-workers* reported similar accumulation dynamics for another ^{68}Ga-labelled cyclodextrin compound ([^{68}Ga]Ga-NODAGA-RAMEB) with BxPC-3 SUV values slightly dropping from 0.45±0.06 at 10 min to 0.14±0.04 at 90 min (Trencsényi et al., 2020).

In addition, increasing T/M values were registered until the 180BxPC-3min time-point favouring clear lesion detection even hours after tracer injection (Fig. 1 **Panel C**), which correlated with *ex vivo* tumor-to-off-target ratios (Fig. 2 **Panel C**). Tracking image contrast over such a long-time interval would not have been possible with a short-lived isotope as ^{68}Ga, therefore to ensure extended T/M monitoring and to specify cyclodextrin pharmacokinetics we chose ^{52}Mn for radiolabelling purposes. Using B16F10 tumors, however, ^{52}Mn-labelled RAMEB presented decreasing T/M values over a similar experimental period (Képes et al., 2024) that contrasted with the current findings. Table 1 shows the *in vivo* tumor-to-off-target ratios at multiple time-points.

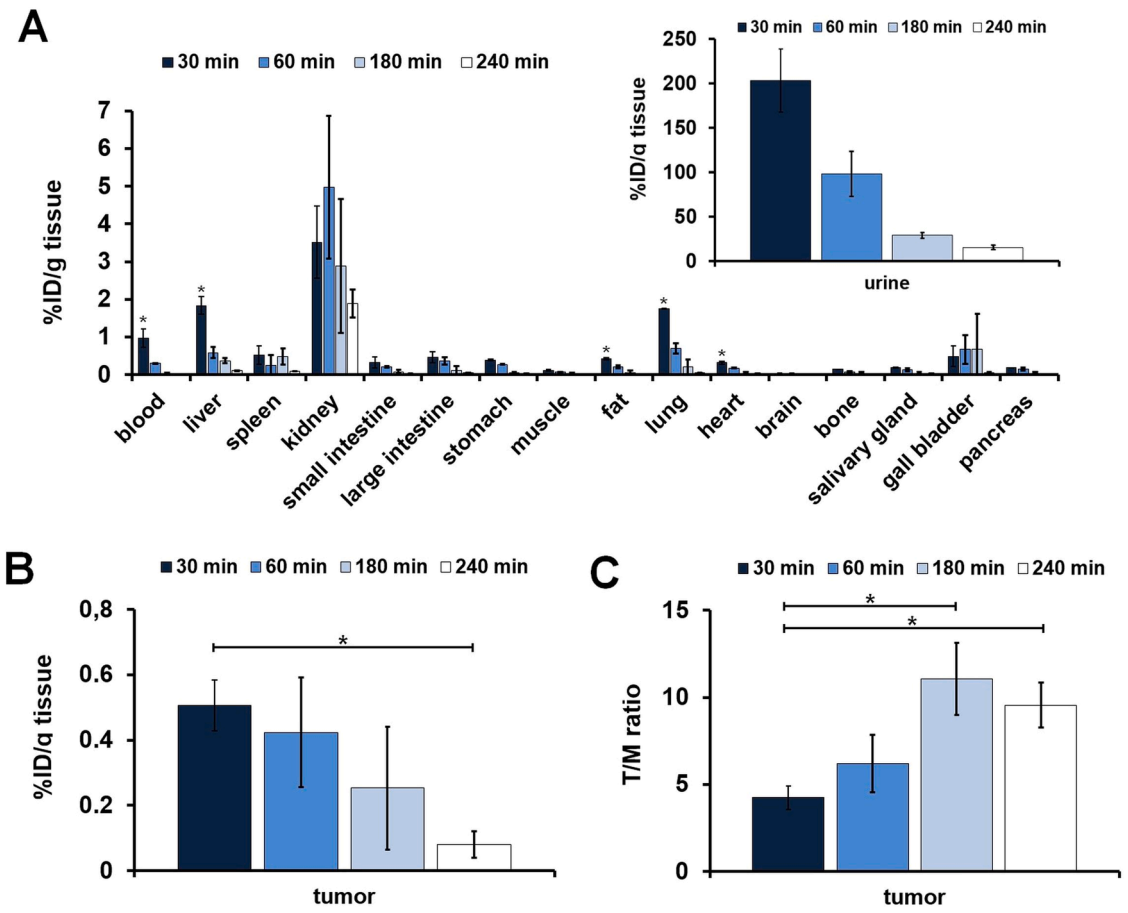

Fig. 2. Ex vivo biodistribution data on [^{52}Mn]Mn-DOTAGA-RAMEB. Time-dependent comparative analysis of ex vivo biodistribution data (%ID/g tissue) of [^{52}Mn]Mn-DOTAGA-RAMEB in healthy control (panel A) and BxPC-3 tumor-bearing (Panel B and C) CB17 SCID mice. Significance level between the 30-min data and the three other investigation time points $p \leq 0.01$ (*) (Panel A). Significance level Panel B and C: $p \leq 0.01$ (*). n = 3 mice/time point. Data are presented as mean±SD. SCID: severe combined immunodeficient, SD: standard deviation.

Considering the findings above, we conclude that despite variations in chelator (DOTAGA vs. NODAGA) or the radionuclide (^{52}Mn vs. ^{68}Ga), all cyclodextrin radiopharmaceuticals consistently demonstrated decreasing BxPC-3 tumor uptake over time, however, depending on the type of the labelling entity meaningful differences could be discovered between their wash-out dynamics. Even if knowledge gaps persist regarding the exact reasons behind the varying pharmacokinetics, we suppose that ^{52}Mn may alter the chemical structure of the compound thereby accelerating the already rapid elimination of the targeting moiety (cyclodextrin) from the tumor cells. This shortens tumor retention time to an even greater extent that leads to rapidly decreasing radiotracer concentrations. In addition, changes in PGE2 levels and EP receptor profile during tumor progression or the appearance of necrotic tumor areas with lower PGE2/EP expression could also be responsible for the decreasing radiotracer uptake.

In agreement with what was observed by Képes et al. with B16-F10 models, our BxPC-3 tumors also exhibited heterogenous uptake pattern at 60-min, although less pronounced than in case of the melanoma xenografts (Képes et al., 2024).

Similarly to other radiolabelled cyclodextrin compounds (Hajdu et al., 2019; Trencsényi et al., 2020), rapid renal clearance of [^{52}Mn]Mn-DOTAGA-RAMEB was evidenced by prompt kidney uptake peaking at the 30–40 min and declining thereafter (Fig. 1 **Panel A**). Apart from the urinary tract, small radioactivity was registered for the other organs and tissues (Fig. 1 **Panel A**), that also aligns with previous findings on cyclodextrin PET probes (Csige et al., 2022; Trencsényi et al., 2020). Nevertheless, minimal off-target uptake favours lesion detection, the presence of physiologically high activities in the urinary organs may constrain the investigation of contiguous structures.

Based on our *in vivo* findings, using [^{52}Mn]Mn-DOTAGA-RAMEB for PET diagnostics may have clear added value in oncological diagnostics. The heterogenous tumor uptake suggests the presence of hypoxic intratumoral regions, indicating the potential of [^{52}Mn]Mn-DOTAGA-RAMEB to differentiate between viable and necrotic tumor areas, which may have future therapeutic implications. Further, given the firm association between tracer accumulation and EP/PGE2 pattern, imaging with [^{52}Mn]Mn-DOTAGA-RAMEB could provide a correct picture on tumor aggressiveness and biological characteristics.

3.3. Post imaging organ distribution studies

The biodistribution and tumor uptake of [^{52}Mn]Mn-DOTAGA-RAMEB were evaluated in healthy and BxPC-3 xenotransplanted CB17 SCID mice (Fig. 2). The uptake values of the tumor and the key organs are displayed in Table 2 and Table 3**. Supplementary Table S1** presents tumor-to-organ ratios.

Corresponding to the PET data, gamma counting showed strong and specific tumor uptake already 30 min post tracer injection (0.51±0.08 % ID/g), confirming the detection capacity of [^{52}Mn]Mn-DOTAGA-RAMEB for BxPC-3 tumors (Fig. 2 and Table 2), consistent with prior *ex vivo* findings (Csige et al., 2022; Szabó et al., 2023).

Followed by the 30BxPC-3min peak uptake, gradually decreasing tumor accumulations were observed until the 240-min time point indicating rapid wash-out kinetics (0.42±0.17, 0.25±0.19 and 0.08±0.04 %

Table 2
Ex vivo uptake (%ID/g) of [^{52}Mn]Mn-DOTAGA-RAMEB in BxPC-3 tumor-bearing CB17 SCID mice (n = 3/time point). Significance level between the 30 min and 240 min data: $p \leq 0.01$ (*). Data are presented as mean±SD.

	[^{52}Mn]Mn-DOTAGA-RAMEB (%ID/g)			
	30 min	60 min	180 min	240 min
BxPC-3	0.51±0.08*	0.42±0.17	0.25±0.19	0.08±0.04
T/M ratio	4.24±0.67*	6.18±1.65	11.06±2.09	9.56±1.30

SCID: severe combined immunodeficient, SD: standard deviation.

Table 3
Ex vivo biodistribution data (%ID/g) of [^{52}Mn]Mn-DOTAGA-RAMEB in healthy control CB17 SCID mice (n = 3/time point). Significance level between the 30-min data and the three other investigation time points: $p \leq 0.01$ (*). Data are presented as mean±SD.

	[^{52}Mn]Mn-DOTAGA-RAMEB (%ID/g)			
	30 min	60 min	180 min	240 min
blood	0.97±0.25*	0.30±0.01	0.03±0.02	0.01±0.01
liver	1.84±0.23*	0.59±0.15	0.38±0.07	0.10±0.02
spleen	0.52±0.24	0.25±0.27	0.48±0.21	0.09±0.01
kidney	3.52±0.95	4.97±1.89	2.88±1.78	1.90±0.37
small intestines	0.33±0.14	0.22±0.02	0.08±0.05	0.03±0.01
large intestines	0.46±0.15	0.37±0.09	0.11±0.11	0.05±0.01
stomach	0.39±0.02	0.27±0.01	0.05±0.02	0.03±0.01
muscle	0.12±0.03	0.07±0.01	0.02±0.02	0.01±0.01
fat	0.42±0.03*	0.21±0.04	0.05±0.06	0.01±0.01
lung	1.75±0.01*	0.70±0.14	0.22±0.20	0.05±0.01
heart	0.32±0.04*	0.18±0.01	0.04±0.03	0.02±0.01
brain	0.04±0.01	0.03±0.01	0.01±0.01	0.00±0.01
bone (femur)	0.14±0.01	0.08±0.01	0.03±0.04	0.01±0.01
salivary gland	0.19±0.01	0.14±0.04	0.04±0.03	0.02±0.01
gall bladder	0.49±0.27	0.68±0.38	0.69±0.92	0.06±0.02
pancreas	0.18±0.01	0.16±0.04	0.04±0.04	0.02±0.01
urine	203.50±35.61	98.24±25.34	29.15±3.10	15.50±2.58

SCID: severe combined immunodeficient, SD: standard deviation.

ID/g 60, 90, and 240 min post [^{52}Mn]Mn-DOTAGA-RAMEB injection, Table 2), which is consistent with our previous stability results on this probe (Képes et al., 2024). This clearance pattern is also in line with earlier reports on radiolabelled cyclodextrins, regardless of the isotope used ([^{68}Ga], [^{213}Bi], Trencsényi et al., 2020; Csige et al., 2022). Although independent of the type of the radioisotope all cyclodextrin probes demonstrated rapid elimination kinetics, there were differences between their accumulations even at the same measurement time points (Csige et al., 2022; Trencsényi et al., 2020). Thus, we suggest that the pharmacokinetics appear to be primarily influenced by the labelling radionuclide, however, the inherent characteristics of the cyclodextrins themselves could also be responsible for the varying uptake mechanisms.

Ex vivo biodistribution data indicating high renal and urinary uptake validated PET results and excretion through the kidneys (Fig. 2 and Table 3). This was further confirmed by blood activities with high value at the earliest time point (30 min: 0.97±0.25 %ID/g) that after a sharp drop 60 min post injection (0.03±0.01 %ID/g) decreased to a minimum until termination (240 min: 0.01±0.01 %ID/g), and this was similar to recent *ex vivo* findings on melanoma models with the same ^{52}Mn-labelled PET agent (Képes et al., 2024).

In contrast to other organs, 30 min post [^{52}Mn]Mn-DOTAGA-RAMEB injection the liver and the lungs showed relatively high initial uptake with decreasing values over time (30-min %ID/g data: 1.84±0.23 and 1.75±0.01 for the liver and the lungs; respectively). Corresponding to previous observations (Hajdu et al., 2019; Képes et al., 2024) these findings may have association with clearance via the gastrointestinal tract and permanent retention of cyclodextrins in aqueous lung territories. Nevertheless, elevated pulmonary and hepatic uptakes were only detected at early time point, such high activities may hamper lesion identification in the close proximity of the corresponding organs. Similarly to what was observed *in vivo*, the same applies for the urinary tract due to the presence of high physiological activity.

Furthermore, *ex vivo* data for the other harvested organs/tissues revealed discrete and sharply declining radioconcentrations over time (Fig. 2 and Table 3), that was similar to prior experiences with radiolabelled cyclodextrins (Csige et al., 2022; Trencsényi et al., 2020).

Even if the registered tumor uptakes with faint off-target activity lead to increasing tumor-to-noise ratios over time (Tabel 1 and Table 2), pharmacokinetical optimization seems straightforward to increase tumor retention. More stable and permanent tumor accumulations would allow better exploitation of the long half-life of ^{52}Mn, supporting delayed imaging. Acquisition at later time points would not only envisage visualization of lesions not seen on early scans but also allow for an even deeper understanding of the uptake mechanism of cyclodextrin molecules.

3.4. Limitations

Even if we successfully identified a target-specific radiotracer to detect tumors with high PGE2 expression, some limitations should be acknowledged. Correction for multiple comparisons was not applied when analyzing across time points. Furthermore, as this work was primarily intended as a proof-of-concept, radiation dose estimation was not included and will be required prior to potential clinical translation.

4. Conclusion

Overall, in this study the long half-life of ^{52}Mn enabled us to characterize the pharmacokinetics of cyclodextrin molecules using preclinical tumor models of pancreatic carcinoma and PET technique. Even though numerous open questions remain to be uncovered, deeper insights into the pharmacokinetics, uptake mechanisms and tumor-homing ability of radiolabelled cyclodextrin derivatives may widen existing knowledge on such oligosaccharides.

In addition, both *in vivo* and *ex vivo* biodistribution data collectively verify the feasibility of ^{52}Mn-labelled RAMEB to identify PGE2 expressing pancreatic cancer, suggesting its possibility to expand the diagnostic armamentarium of malignancies with high PGE2 expression. Moreover, the current findings may also initiate the establishment of additional cyclodextrin PET agents that is critical to the maximum benefit of patients with oncological diseases.

Considering the advantages of ^{52}Mn over well-established isotopes, our results may also propose its use for radiolabelling purposes. First, its long decay half-life gives enough room for radiosynthesis and related work-up processes including target separation, conjugation or labelling. Second, long-lived ^{52}Mn allows for centralized distribution and delivery to facilities far from isotope production sites. Additionally, using ^{52}Mn prolonged acquisition time (Omweri et al., 2024) is guaranteed, that favours the visualization of such alterations that may not be apparent on PET examinations covering imaging periods of only a few hours. Later time-point acquisition reveals lesions missed on early scans, resulting in better diagnostic accuracy. Finally, given its low average positron energy (242 keV) and suitable positron branching ratio (29.6 %) using ^{52}Mn-labelled compounds high-resolution PET images could be obtained (Brandt et al., 2019; Fonslet et al., 2017; Omweri et al., 2024).

In summary, [^{52}Mn]Mn-DOTAGA-RAMEB may herald a new era in cancer diagnostics, however, constraints around its pharmacokinetics pose issues for translation into clinical settings. Additionally, limitations related to the challenge of lesion detection near the lungs and the liver must also be addressed.

Funding

The authors declare financial support was received for the research, authorship, and/or publication of this article. The project no. TKP2021-NKTA-34 has been implemented with the support provided by the Ministry of Culture and Innovation of Hungary from the National Research, Development and Innovation Fund, financed under the TKP2021-NKTA funding scheme (E.M.). The research was also supported by the University of Debrecen Program for Scientific Publication (A.F.) and by the OTKA K-147,308 research grant of the National Research, Development and Innovation Office, Budapest, Hungary (F. F.).

Data availability statement

The dataset used and/or analyzed during the current study are available from the corresponding author on reasonable request.

CRediT authorship contribution statement

Renáta Adél Dienes: Visualization, Methodology, Investigation, Data curation. **Lili Anna Komor:** Visualization, Methodology, Investigation, Data curation. **Judit P. Szabó:** Methodology, Investigation. **András Berzi:** Investigation, Funding acquisition. **Miklós Emri:** Investigation, Funding acquisition. **Dezső Szikra:** Methodology, Data curation. **Anikó Fekete:** Validation, Investigation, Funding acquisition. **Gábor Opposits:** Validation, Software, Methodology, Data curation. **István Jószai:** Validation, Methodology, Investigation, Formal analysis. **István Kertész:** Investigation, Formal analysis, Data curation. **Ferenc Fenyvesi:** Visualization, Validation, Supervision. **György Trencsényi:** Writing – review & editing, Writing – original draft, Visualization, Validation, Resources, Project administration. **István Hajdu:** Writing – review & editing, Writing – original draft, Validation, Supervision, Conceptualization. **Zita Képes:** Writing – review & editing, Writing – original draft, Validation, Supervision, Conceptualization.

Declaration of competing interest

The authors declare no conflict of interest.

Acknowledgements

None.

Supplementary materials

Supplementary material associated with this article can be found, in the online version, at doi:10.1016/j.ejps.2025.107344.

References

Ahenkorah, S., Cassells, I., Deroose, C.M., Cardinaels, T., Burgoyne, A.R., Bormans, G., Ooms, M., Cleeren, F., 2021. Bismuth-213 for targeted radionuclide therapy: from atom to bedside. Pharmaceutics 13, 599. https://doi.org/10.3390/pharmaceutics13050599.

Brandt, M., Cardinale, J., Rausch, I., Mindt, T.L., 2019. Manganese in PET imaging: opportunities and challenges. J. Lab. Comp. Radiopharm. 62, 541–551. https://doi.org/10.1002/jlcr.3754.

Csige, K., Szabó, J.P., Kálmán-Szabó, I., Dénes, N.S., Szikra, D., Képes, Z., Opposits, G., Méhes, G., Kertész, I., Fenyvesi, F., Trencsényi, G., Hajdu, I., 2022. In vivo investigation of Gallium-68 and Bismuth-205/206 labeled beta cyclodextrin for targeted alpha therapy of prostaglandin E2 receptor-expressing tumors in mice. Int. J. Pharm. 625, 122132. https://doi.org/10.1016/j.ijpharm.2022.122132.

Fang, H.Y., Lin, T.S., Lin, J.P., Wu, Y.C., Chow, K.C., Wang, L.S., 2003. Cyclooxygenase-2 in human non-small cell lung cancer. Eur. J. Surg. Oncol. 29, 171–177. https://doi.org/10.1053/ejso.2002.1316.

Finetti, F., Terzuoli, E., Giachetti, A., Santi, R., Villari, D., Hanaka, H., Radmark, O., Ziche, M., Donnini, S., 2015. MPGES-1 in prostate cancer controls stemness and amplifies epidermal growth factor receptor-driven oncogenicity. Endocr. Relat. Cancer 22, 665–678. https://doi.org/10.1530/ERC-15-0277.

Finetti, F., Travelli, C., Ercoli, J., Colombo, G., Buoso, E., Trabalzini, L., 2020. Prostaglandin E2 and cancer: insight into tumor progression and immunity. Biology 9, 434. https://doi.org/10.3390/biology9120434.

Fonslet, J., Tietze, S., Jensen, A.I., Graves, S.A., Severin, G.W., 2017. Optimized procedures for manganese-52: production, separation and radiolabeling. Appl. Radiat. Isot. 121, 38–43. https://doi.org/10.1016/j.apradiso.2016.11.021.

Giesel, F.L., Adeberg, S., Syed, M., Lindner, T., Jiménez-Franco, L.D., Mavriopoulou, E., Staudinger, F., Tonndorf-Martini, E., Regnery, S., Rieken, S., El Shafie, R., Röhrich, M., Flechsig, P., Kluge, A., Altmann, A., Debus, J., Haberkorn, U., Kratochwil, C., 2021. FAPI-74 PET/CT using either ^{18}F-AlF or cold-kit ^{68}Ga labeling: biodistribution, radiation dosimetry, and tumor delineation in lung cancer patients. J. Nucl. Med. 62, 201–207. https://doi.org/10.2967/jnumed.120.245084.

Graves, S.A., Hernandez, R., Fonslet, J., England, C.G., Valdovinos, H.F., Ellison, P.A., Barnhart, T.E., Elema, D.R., Theuer, C.P., Cai, W., Nickles, R.J., Severin, G.W., 2015. Novel preparation methods of (52)Mn for ImmunoPET imaging. Bioconjug. Chem. 26, 2118–2124. https://doi.org/10.1021/acs.bioconjchem.5b00414.

Hajdu, I., Angyal, J., Szikra, D., Kertész, I., Malanga, M., Fenyvesi, É., Szente, L., Vecsernyés, M., Bácskay, I., Váradi, J., Fehér, P., Ujhelyi, Z., Vasvári, G., Rusznyák, Á., Trencsényi, G., Fenyvesi, F., 2019. Radiochemical synthesis and preclinical evaluation of 68Ga-labeled NODAGA-hydroxypropyl-beta-cyclodextrin (68Ga-NODAGA-HPBCD). Eur. J. Pharm. Sci. 128, 202–208. https://doi.org/10.1016/j.ejps.2018.12.001.

Half, E., Tang, X.M., Gwyn, K., Sahin, A., Wathen, K., Sinicrope, F.A., 2002. Cyclooxygenase-2 expression in human breast cancers and adjacent ductal carcinoma in situ. Cancer. Res. 62, 1676–1681.

Hanahan, D., Weinberg, R.A., 2011. Hallmarks of cancer: the next generation. Cell 144, 646–674. https://doi.org/10.1016/j.cell.2011.02.013.

Hirayama, F., Kurihara, M., Uekama, K., 1984. Improving the aqueous stability of prostaglandin E2 and prostaglandin A2 by inclusion complexation with methylated-beta-cyclodextrins. Chem. Pharm. Bull/ 32, 4237–4240. https://doi.org/10.1248/cpb.32.4237.

Képes, Z., Szabó, J.P., Kálmán-Szabó, I., Sass, T., Esze, R., Opposits, G., Jószai, I., Szikra, D., Fenyvesi, F., Hajdu, I., Trencsényi, G., 2024. ^{52}Mn-labelled beta-cyclodextrin for Melanoma imaging: a proof-of-concept preclinical study. In. vivoin. Vivo. (Brooklyn) 38, 2591–2600. https://doi.org/10.21873/invivo.13735.

Niu, J.C., Ma, N., Liu, W., Wang, P.J., 2019. EP1 receptor is involved in prostaglandin E2-induced osteosarcoma growth. Bosn. J. Basic. Med. Sci. 19, 265–273. https://doi.org/10.17305/bjbms.2019.4177.

Omweri, J.M., Saini, S., Houson, H.A., Tekin, V., Pyles, J.M., Parker, C.C., Lapi, S.E., 2024. Development of ^{52}Mn labeled Trastuzumab for extended time point PET imaging of HER2. Mol. ImAging. Biol. 26, 858–868. https://doi.org/10.1007/s11307-024-01948-4.

Panza, E., de Cicco, P., Ercolano, G., Armogida, C., Scognamiglio, G., Anniciello, A.M., Botti, G., Cirino, G., Ianaro, A., 2016. Differential expression of cyclooxygenase-2 in metastatic melanoma affects progression free survival. Oncotarget 7, 57077–57085. https://doi.org/10.18632/oncotarget.10976.

Pyles, J.M., Omweri, J.M., Lapi, S.E., 2023. Natural and enriched Cr target development for production of Manganese-52. Sci. Rep. 13, 1167. https://doi.org/10.1038/s41598-022-27257-w.

Santiso, A., Heinemann, A., Kargl, J., 2024. Prostaglandin E2 in the tumor microenvironment, a convoluted affair mediated by EP receptors 2 and 4. Pharmacol. Rev. 76, 388–413. https://doi.org/10.1124/pharmrev.123.000901.

Sauer, R.S., Rittner, H.L., Roewer, N., Sohajda, T., Shityakov, S., Brack, A., Broscheit, J. A., 2017. A novel approach for the control of inflammatory pain: prostaglandin E2 complexation by randomly methylated β-cyclodextrins. Anesth. Analg. 124, 675–685. https://doi.org/10.1213/ANE.0000000000001674.

Szabó, J.P., Csige, K., Kálmán-Szabó, I., Arató, V., Opposits, G., Jószai, I., Kertész, I., Képes, Z., Méhes, G., Fenyvesi, F., Hajdu, I., Trencsényi, G., 2023. In vivo assessment of tumor targeting potential of ^{68}Ga-labelled randomly methylated beta-cyclodextrin (RAMEB) and 2-hydroxypropyl-β-cyclodextrin (HPβCD) using positron emission tomography. Int. J. Pharm. 630, 122462. https://doi.org/10.1016/j.ijpharm.2022.122462.

Takahashi, H., Uehara, H., Ogawa, H., Umemoto, H., Bando, Y., Izumi, K., 2015. Inhibition of EP2/EP4 signaling abrogates IGF-1R-mediated cancer cell growth: involvement of protein kinase C-θ activation. Oncotarget 6, 4829–4844. https://doi.org/10.18632/oncotarget.3104.

Tong, D., Liu, Q., Wang, L.A., Xie, Q., Pang, J., Huang, Y., Wang, L., Liu, G., Zhang, D., Lan, W., Jiang, J., 2018. The roles of the COX2/PGE2/EP axis in therapeutic resistance. Cancer. Met. Rev. 37, 355–368. https://doi.org/10.1007/s10555-018-9752-y.

Trencsényi, G., Kis, A., Szabó, J.P., Ráti, Á., Csige, K., Fenyvesi, É., Szente, L., Malanga, M., Méhes, G., Emri, M., Kertész, I., Vecsernyés, M., Fenyvesi, F., Hajdu, I., 2020. In vivo preclinical evaluation of the new 68Ga-labeled beta-cyclodextrin in prostaglandin E2 (PGE2) positive tumor model using positron emission tomography. Int. J. Pharm. 576, 118954. https://doi.org/10.1016/j.ijpharm.2019.118954.

Yip-Schneider, M.T., Barnard, D.S., Billings, S.D., Cheng, L., Heilman, D.K., Lin, A., Marshall, S.J., Crowell, P.L., Marshall, M.S., Sweeney, C.J., 2000. Cyclooxygenase-2 expression in human pancreatic adenocarcinomas. Carcinogenesis 21, 139–146. https://doi.org/10.1093/carcin/21.2.139.